Permanent Magnet Electrodynamic Suspensions Applied to MAGLEV Transportation Systems: A Review

Louis Beauloye and Bruno Dehez, *Senior Member, IEEE*

***Abstract*— This article reviews permanent magnet electrodynamic suspensions (PM-EDSs) used in ground transportation systems, such as Magnetic Levitation (MAGLEV) trains. The different suspension topologies are first presented, considering separately their two main components, namely the track and the magnetic field source. Beyond that, a phenomenological explanation of the evolution with the speed of the drag and levitation forces is provided, depending on the track topology. The models aimed at predicting the behavior and performance of the suspension are then detailed, classifying them according to whether they are global or local. Finally, the main experimental setups developed to validate PM-EDSs are described.**

***Index Terms*— Electrodynamic, electrodynamic suspension (EDS), Magnetic Levitation (MAGLEV), permanent magnet (PM), suspension.**

I. Introduction

THE energy consumption and greenhouse gas emissions associated with long-distance trips are becoming more and more significant [1]. Indeed, the average number of kilometers traveled by people continues to grow, the share of long-distance trips in this number of kilometers is also increasing, and the trend is to seek to reduce travel times by increasing the speed of the means of transport used. Magnetic Levitation (MAGLEV) systems which are known for several decades seem to be good candidates to overcome these challenges. Recently, they regained interest due to Elon Musk's announcement of the Hyperloop [2] as they could be integrated into this high-speed ground transportation [3]. Relying on the principle of magnetic levitation, these systems remove the friction between the wheels and the rail in conventional railways allowing them to reach higher speeds and to consume less power. They also present numerous advantages such as reduced wear and maintenance costs, less noise and vibrations, and quicker acceleration and deceleration [4].

Manuscript received 24 March 2022; revised 10 June 2022; accepted 15 July 2022. Date of publication 21 July 2022; date of current version 21 February 2023. *(Corresponding author: Louis Beauloye.)*

Louis Beauloye is with the Mechatronic, Electrical Energy, and Dynamic Systems Department (MEED), Institute of Mechanics, Materials and Civil Engineering (IMMC), Université catholique de Louvain (UCLouvain), 1348 Louvain-la-Neuve, Belgium, and also is a Research Fellow of the Fonds de la Recherche Scientifique - FNRS (e-mail: louis.beauloye@uclouvain.be).

Bruno Dehez is with the Mechatronic, Electrical Energy, and Dynamic Systems Department (MEED), Institute of Mechanics, Materials and Civil Engineering (IMMC), Université catholique de Louvain (UCLouvain), 1348 Louvain-la-Neuve, Belgium (e-mail: bruno.dehez@uclouvain.be).

Digital Object Identifier 10.1109/TTE.2022.3193296

These technologies encompass several aspects being the propulsion, the levitation, and the guidance. Lee *et al.* [4] reviewed these three technological aspects as well as worldwide MAGLEV train projects. The propulsion is provided by a linear motor such as the linear induction motor (LIM) or linear synchronous motor (LSM) [5]. The levitation can be achieved using either an attractive force in *electromagnetic suspensions* (EMSs), a repulsive force in *electrodynamic suspensions* (EDSs), or a combination of the two with a hybrid suspension [6] or in *high-temperature superconducting* (HTS) *maglev* [7], [8]. EMS uses electromagnets acting on a ferromagnetic rail while EDS relies on a passive magnetic field source and a conductive guideway. HTS maglev is based on the flux-pinning effect of type-II superconductors above a permanent magnet (PM) guideway. The guidance, preventing a lateral displacement of the vehicle, can also be generated using either an attractive or a repulsive force. There exist technologies integrating the propulsion, guidance, and levitation as summarized by Bird [9]. This could reduce costs but at the expense of the complexity of the design.

EDSs are fully passive and therefore do not require to control the air gap between the guideway and the vehicle as in EMSs. This is attractive since accurate control can be challenging to ensure the stability of the inherently unstable EMS systems [10]. Besides, the passive characteristic of EDSs implies that they are fail-safe and more reliable, contrary to EMSs [11].

As reviewed by França *et al.* [12], the magnetic field source of EDSs can be either superconducting magnets (SCMs) or PMs. Superconductors are more difficult to use as they need a complex and expensive device for cooling. With the advent of rare-earth magnets, PMs can produce a magnetic field sufficiently large to ensure the levitation of MAGLEV vehicles. Therefore, for their simplicity and robustness, this work focuses on permanent magnet electrodynamic suspensions (PM-EDSs). PM-EDSs, and more generally EDSs, can not achieve levitation at low speed. This implies the use of mechanical wheels which can also provide a large air gap, reducing eddy current losses where these are dominant. PM-EDSs are investigated for various applications. However, there exist very few full-scale tests and real integrations of this suspension in transportation systems. The General Atomics Urban Maglev Program developed a low-speed MAGLEV based on PM-EDS and tested it on a full-scale

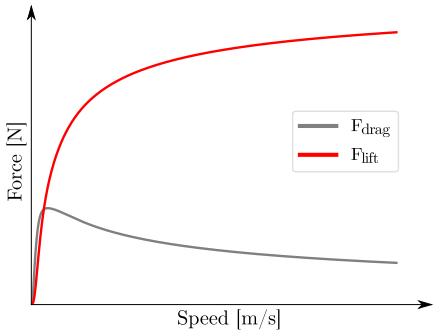

Fig. 1. Typical speed dependence of the lift and drag forces of an EDS.

test track [13]. Other works are focused on high-speed transportation systems such as the Hyperloop [14]. Besides, student teams participating in the SpaceX Hyperloop Pod Competition have built a pod equipped with PM-EDSs [15].

The dynamic behavior of EDSs is quite complex but important to predict because of the stability issues they face, as reviewed by Rote and Cai [16]. Different topologies were studied to reach better stability, e.g., with damper coils [17], active magnets [18], or coils wounded around the magnets [19].

In this context, this article aims at providing a review of PM-EDS topologies, and their modeling with a focus on quasi-static performance. Its structure is the following. In Section II, the working principle, as well as the criteria allowing to compare the different EDSs, are explained. In Section III, the existing topologies are presented, considering separately the track and the magnetic field source, without taking into account the features specifically developed to address the stability issues. A deeper explanation of the forces generated in EDSs is given depending on the type of track. In Section IV, the models either global or local, and either analytical or numerical, used to compute the force in PM-EDSs are developed. Simple scaling laws of one of the main criteria, the so-called lift-to-drag ratio (LDR), are also summarized. Finally, an overview of some of the experimental setups from the literature is given in Section V.

II. Working Principle and Criteria

PM-EDSs are made of PMs moving with respect to a fixed conductive guideway separated by an air gap. The moving magnetic field from the PMs induces eddy currents in the conductor, which react with the magnetic field that produced them to create a force. This force has two components, one in the levitation direction, named levitation, suspension or lift force, and one in the opposite direction of the movement, named drag force. As illustrated in Fig. 1, the former increases monotonically with speed but tends asymptotically toward a maximum value, while the latter increases before reaching a maximum and decreasing monotonically. An explanation of this behavior is given in Section III.

Two important parameters are widely used in the literature to assess the performance of such systems. The first one is the lift-to-drag ratio, noted LDR, which is an indicator of the efficiency of the suspension at a given speed

$$\mathrm{LDR} = \frac{F_{\mathrm{lift}}}{F_{\mathrm{drag}}}. \tag{1}$$

The second one is the lift-to-weight ratio, noted LWR, which represents the amount of lift force that can be obtained from a given volume or weight of PM

$$\mathrm{LWR} = \frac{F_{\mathrm{lift}}}{W_{\mathrm{PM}}}. \tag{2}$$

Other parameters and ratios were defined in the literature, such as the ratio between the lift force and the cost of the PMs or the ratio between the PM weight and the square of the magnetic flux, but they can be related either to the LDR or to the LWR. The optimization of these criteria separately leads to different solutions in terms of geometry [20], [21]. Indeed, the LWR is linked to the PM volume and thus cost for a given application whereas the LDR is more related to the efficiency of the system and thus the operation. The use of the LWR rather than the LDR depends therefore on the targeted application. Both criteria could also be included in global criteria able to encompass more aspects of the suspension and the application such as the load [22] or the speed profile [14].

III. Topologies

The different topologies of PM-EDSs can be classified depending on their magnetic field source and their track, also referred to as guideway as represented in Fig. 2. These constitute two distinct elements of PM-EDSs. It is then possible to combine nearly all the topologies of both parts together to form a PM-EDS, which justifies presenting them separately.

A. Track

The track is either discrete or continuous. Discrete tracks [see Fig. 3(a)–(c)] are built from discrete conductive loops connected [see Fig. 3(c)] or not [see Fig. 3(a) and (b)] to each other, whereas continuous tracks [see Fig. 3(d) and (e)] are made of a homogeneous sheet of conductive material such as aluminum or copper. Discrete tracks can be seen as tracks having a periodic electrical resistivity along the translational direction x, which is invariant in continuous tracks [23].

1) Discrete Tracks: The behavior of the forces with the speed illustrated in Fig. 1 can be easily explained for this type of track. The conductive loops can be represented with an equivalent circuit depicted in Fig. 4 with R and L their global resistance and inductance and E the induced back-electromotive force. On this basis, the drag and lift forces can be expressed from the active and reactive powers as

$$F_{\mathrm{drag}} = \frac{P}{v} = \frac{1}{v}\frac{E^2 R}{R^2 + (\omega L)^2} \tag{3}$$

$$F_{\mathrm{lift}} = \frac{Q}{v} = \frac{1}{v}\frac{E^2 \omega L}{R^2 + (\omega L)^2} \tag{4}$$

where $\omega = v(\pi/\tau)$, v is the translational speed, and τ is the pole pitch of the magnetic field source. From [10] and [24], it can indeed be deduced that the lift force is equal to the ratio between the reactive power Q and the speed. Because the back-electromotive force E is proportional to the speed, the drag and lift forces follow the asymptotic behavior summarized in Table I. Or, in other words, when the speed is low and the resistive effects prevail, the back-electromotive force E and the resulting current are in phase. The power absorbed by the track is mainly active and corresponds

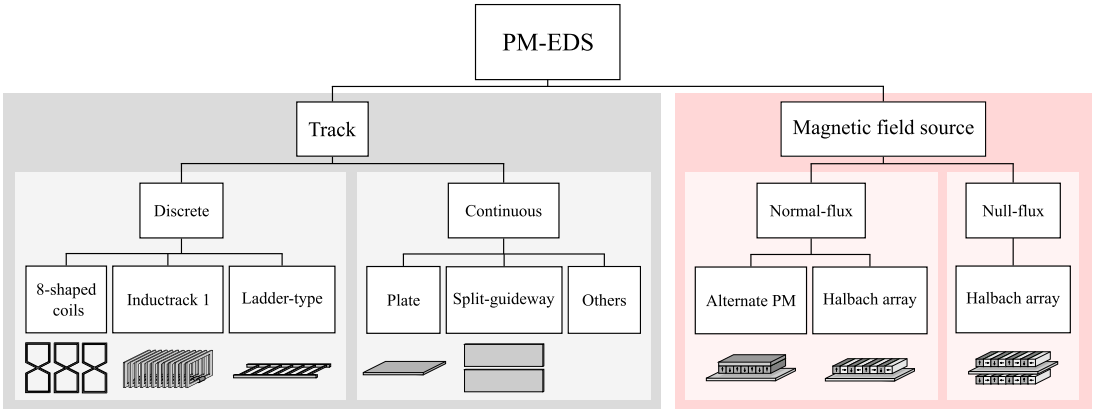

Fig. 2. Classification of the existing track and magnetic field source topologies of PM-EDSs.

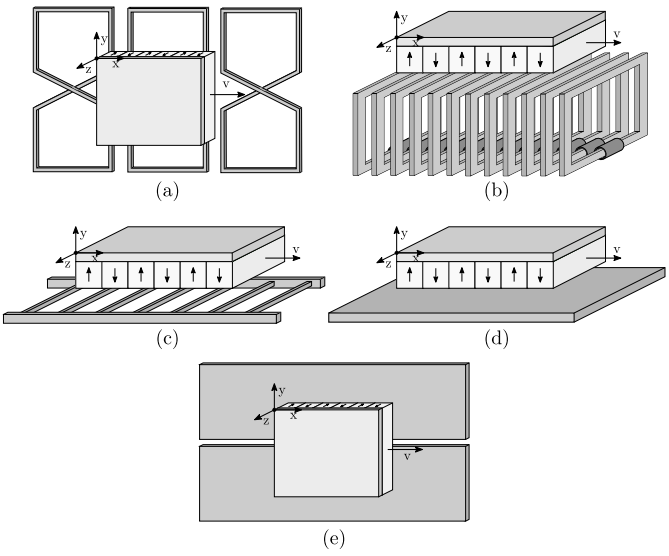

Fig. 3. Track configurations. The y-axis is the lift direction. (a) Discrete, eight-shaped coils. (b) Discrete, array of shorted coils with the inductive loading. (c) Discrete, ladder-type. (d) Continuous, conductive plate. (e) Continuous, split-guideway.

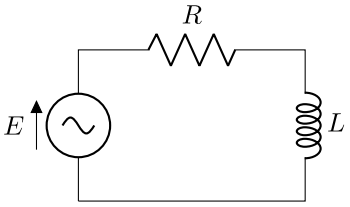

Fig. 4. Equivalent circuit of the discrete track.

TABLE I
ASYMPTOTIC BEHAVIOR OF THE FORCES

Low speed	High speed
$F_{drag} \propto v$	$F_{drag} \propto v^{-1}$
$F_{lift} \propto v^2$	$F_{lift} \propto 1$

mechanically to the drag force that opposes the movement. This force, therefore, increases with the speed as both the induced voltage and the resulting current are proportional to the speed. Inversely, when the inductive effects are dominant at high speed, the voltage and the current are shifted by 90 electrical degrees leading mainly to reactive power and thus a maximum lift force and very low losses. In between, as expressed by Galluzzi *et al.* [24] and Van Verdeghem *et al.* [25], the current can be separated into two components, one in phase with the magnetic flux linkage, generating lift, and one in quadrature, generating drag. An increase in the inductive effects leads to a faster rise of the lift force which thus settles at a lower speed. This implies a higher LDR but also a higher impedance, which leads to lower currents and smaller drag and lift forces.

Powell and Danby [26] were the first to propose discrete tracks but with a magnetic field source made of SCMs. They introduced the null-flux concept which consists in connecting two coils facing the magnetic field source so that the total flux linked by these coils and, therefore, the total back electromotive forces cancel for a specific position. The advantage of this type of track is having no current and thus no losses when the magnetic field source is centered with regard to the coils. However, the main difference with the other topologies is the need for a shift between the magnetic field source and the track to have induced currents and thus forces. This topology can be side-wall mounted and the coils are shaped like the figure eight. A well-known feature of this topology is its high LDR. According to [27], the drag forces generated by the upper and lower loops indeed nearly cancel each other because the currents go in opposite directions in each loop. Null-flux coils offer also a great guidance force, restoring a lateral displacement of the vehicle. It can be further improved by cross-connecting the null-flux coils on both sides of the vehicle [27]. An in-depth analysis of this topology with SCMs can be found in [28]–[31]. However, it was also studied with PMs in [32]–[35] [see Fig. 3(a)]. As expected, Guo *et al.* [34] showed a higher LDR for a track made of this type of coils than for a continuous track with the same specifications.

At the Lawrence Livermore National Laboratory (LLNL), Post and Ryutov [10], [36] developed the Inductrack, a magnetic levitation system using a close-packed array of

shorted coils in the track, as depicted in Fig. 3(b). These coils have their magnetic axis parallel to the direction of travel. A ferromagnetic material is added around the lower horizontal portion of the coils, far enough from the PMs to avoid an attractive force between the two, to increase the inductive loading and therefore, as suggested above, the LDR. They showed that the Inductrack can have a significantly higher LDR than EDSs with a continuous plate. The lateral stiffness of the suspension in Fig. 3(b) is very low and even negative as stated in [37], and, therefore, a supplementary guiding system must be added. Han [18], Murai and Hasegawa [37], and Wang and Yang [38] studied further the Inductrack technology with different types of simulations and ways of modeling the magnetic field source.

Combined with a novel arrangement of magnets described in Section III-B2, Kratz and Post [39] chose a ladder-type track with the rungs made from Litz wire shorted at their ends with massive copper. This type of wire is used to reduce Ohmic losses at high frequencies and to mitigate the proximity effect. This constitutes the second Inductrack concept and is represented in Fig. 3(c) with a simplified magnetic field source. Yamada *et al.* [40] showed an increase in the LDR for the ladder-type track compared to loop-shaped coils, which are independent coils with their magnetic axis perpendicular to the direction of travel. Akinbiyi *et al.* [41] compared sheet and ladder-type guideways with identical quantities of material in both cases. They concluded that ladder-type tracks can produce slightly higher LDR but continuous tracks have better overall performance in terms of lift force or dynamic stability. Due to their discrete nature, ladder-type tracks will also produce a fluctuation in the forces. This type of track is not stable laterally. This feature will be developed further in Section III-A2 for another type of flat guideway, the continuous conductive plate.

2) Continuous Tracks: The electromagnetic forces of PM-EDS systems with a continuous track show the same evolution with the speed, but the physical explanation is a bit more complex. As in discrete tracks, the resistive part of the impedance of the track dominates at low speed and the main force is the drag force. At high speed, the inductive behavior of the track dominates and only the lift force prevails [14], [42].

The difference between continuous and discrete tracks lies in the diffusion of the magnetic field inside the conductor which has two impacts, being the skin effect and the diffusion angle, both depending on the speed. First, the inductive behavior of the track opposes the change of magnetic field in the conductor, preventing it from entering deeply into the conductor. The skin depth δ_{skin} can be defined as the penetration depth at which the magnetic field amplitude is reduced by a factor e^{-1} [43]

$$\delta_{\text{skin}} = \sqrt{\frac{2\tau}{\pi \mu \sigma v}} \tag{5}$$

where τ is the pole pitch of the magnetic field source, μ is the magnetic permeability of the conductive material, σ is the electric conductivity of the material, and v is the translational speed. The lower the speed, the longer is the skin depth, and the deeper the magnetic field and the currents penetrate. Second, in relatively thick plates (see Section IV-B2), the current densities are diffused in the track with a certain angle that depends on the skin depth and thus the speed of the magnetic field source. This angle, impacting the distribution of the currents inside the track, can be seen as a combination between the translational speed and the vertical diffusion of the magnetic field inside the conductor. Both effects are depicted in Fig. 5, which was obtained with a 2-D Fourier-based model (see Section IV-B2) with an ideal Halbach array (see Section III-B). The comparison between both speeds is the point of interest rather than the exact dimensions and numerical values. On the left side, at low speed, the currents go deep inside the conductor. On the right side, at high speed, the currents penetrate much less inside the track and the diffusion angle is greater. The skin depth is represented by the dashed line.

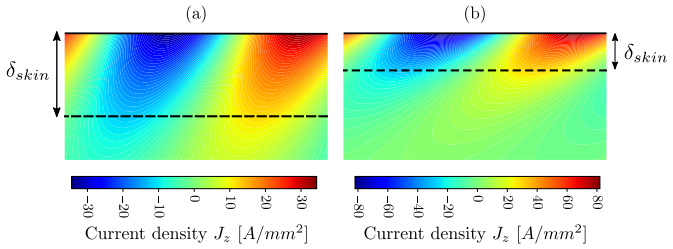

Fig. 5. Eddy current densities in the continuous track. (a) For a speed of 10 m/s. (b) For a speed of 50 m/s. The dashed lines represent the skin depth δ_{skin}.

Hao *et al.* [44] studied the eddy current distribution due to a single coil, being the magnetic field source, moving above a conductive board. They explained how the evolution of the forces with the speed can be linked to the current distribution in the conductive board.

To the authors' best knowledge, all the topologies studied in the past 20 years other than those described before used a continuous conductive plate as track [17], [20]–[22], [24], [45]–[57]. This conductive track can be made of several layers to reduce the eddy currents in the y-axis, thus decreasing the drag force but not the lift force [58]. An exception to the plate can be found in [59] where Guo *et al.* studied a PM-EDS with a split-guideway mounted on the side of the vehicle, illustrated in Fig. 3(e). In this configuration, this topology showed a guidance force significantly higher than the lift force.

Focusing on the lateral guidance, EDSs with flat guideways such as the one in Fig. 3(d), or even in Fig. 3(c) as mentioned in Section III-A1, do not provide sufficient guidance force and are even unstable laterally [60], [61]. For these configurations, either a guiding mechanism such as another PM array mounted on the side of the vehicle must be adopted or an interaction between the propulsion and the levitation devices is also possible to provide a guiding force. Other special track topologies were investigated to enhance the lateral stability of PM-EDSs. Split flat conductive plates can be found in [60] and [62]. This technology could be also useful to induce a lateral restoring force due to a lateral displacement of the PM-EDS. It should be noted that it could also be used with a ladder-type guideway.

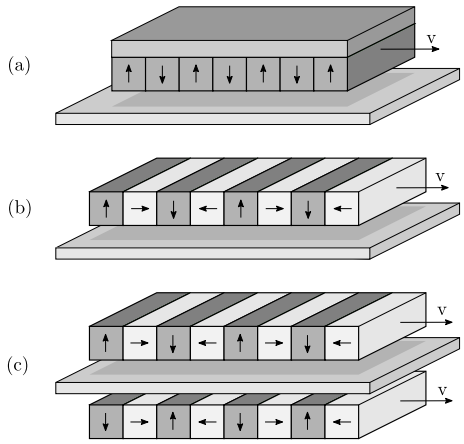

Fig. 6. PMs configurations. (a) *Normal-flux*, alternate poles with back-iron. (b) *Normal-flux*, Halbach array. (c) *Null-flux*, Halbach array.

The guideway can also have a curve shape [63], [64] or a V-shape [65], beneficing from a force directed to the inside of the vehicle but at the cost of a reduced lift force. The curved guideway, or arc-guideway, must be split to have a stable lateral motion [61] but can allow banking of the vehicle.

B. Magnetic Field Source

The magnetic field source in PM-EDSs is an arrangement of PMs. These magnets can be arranged in an alternation of magnetic poles with a back-iron closing the magnetic flux lines or in a Halbach array pattern. This array does not need for a back iron as it strengthens the magnetic field on one side and weakens it on the other one. It is thus widely used in PM-EDSs. Some authors improved the Halbach array for EDS systems. Davey [66] showed, through an optimization, that adding a back-iron of varying thickness behind the magnets can reduce the ratio of the weight of the PMs to the square of the magnetic flux, which can be linked to the LWR. Dimensions and geometries were also optimized in [67]–[69].

During the 1970s, early works studied the arrangement of magnetic field sources with regard to a conductive track [70]–[73]. They used electromagnets since the PMs were not able to produce a sufficient magnetic field at that time. Two PM arrangements are possible for EDS systems: the *normal-flux* and the *null-flux*.

1) Normal-Flux: Only one arrangement of PMs moves above the track [see Fig. 6(a) and (b)]. This topology was studied in most researches except the ones cited in Section III-B2. Flankl *et al.* [21] showed that the drag force decreases with higher rail conductivity and longer pole pitch of the magnetic field source. Hasanzadeh *et al.* [53] found optimum PM dimensions to maximize the ratio of the lift force to the material cost of the PMs and the track. Kublin *et al.* [22] calculated that selecting a fill factor of the Halbach array, i.e., the ratio between the horizontally magnetized PM and the wavelength, different than 0.5 can decrease the power consumption of the levitation system. Through an analytical optimization of the LWR, Hu *et al.* [20] concluded that the optimum wavelength-to-gap and thickness-to-gap ratios of the Halbach array were 4π and $(4\pi/5)$, respectively. Wang *et al.* [57] showed that a ratio of the thickness of the magnet to the pole pitch around 0.4 maximizes the LWR and is rather independent of the pole pitch. According to their results, a ratio of the thickness of the conductive plate to the pole pitch between 0.1 and 0.2 maximizes also the LWR and minimizes the power losses. Among other parametric studies, Guo *et al.* [59] tested three possible arrangements of magnets: a single magnet, the same pole arrangement, and an alternating pole arrangement. They concluded that the last one was better as it developed the highest lift force.

In addition to the linear configuration, the magnets can rotate above the track to generate the eddy currents and thus the forces. In this configuration, called *electrodynamic wheels* (EDWs), both thrust and lift forces can be produced at the same time at the expense of additional motors to induce the rotation. Two topologies of EDWs are possible with axially and radially magnetized PMs arranged in an annular shape. Axial EDWs, with a rotation axis aligned with the y-axis, have the advantage to produce lift force with no translational movement and to have a larger area of interaction between the PMs and the track [74]. However, the propulsion can only be produced with a tilt angle over the track or an overlap between the EDW and the edge of the track [65]. Besides, greater guidance forces can be obtained but with an inclined guideway. Radial EDWs, with a rotation axis aligned with the z-axis, were also extensively investigated [75]–[77]. Bird and Lipo [75] showed a higher LWR for an EDW compared to a PM-EDS made of a nonrotating EDW. More recently, Sang *et al.* [78] investigated experimentally the forces and their evolution with the rotational speed and the air gap.

2) Null-Flux: In this topology, illustrated in Fig. 6(c), two arrangements of PMs are positioned on both sides of the track, with the same magnetic poles facing each other. By superposition, the vertical components of the magnetic flux density, responsible for the drag, counteract each other whereas the horizontal ones, responsible for the lift, reinforce each other. Kratz and Post [39] were the first to transpose this topology to PM-EDSs. They studied experimentally a ladder-type track sandwiched between two Halbach arrays. Chen and Zhang [50] and Chen *et al.* [52] investigated the same topology, but with a continuous track. They showed that the double-sided arrays have a significantly higher LDR but at the cost of a reduced LWR. Based on these results, Duan *et al.* [55] optimized an asymmetrical topology with a multiobjective algorithm. By adjusting the height ratio ε between the upper and lower arrays, they selected a trade-off along the Pareto front between maximum LDR in the symmetrical double-sided geometry ($\varepsilon = 0.5$) and maximum LWR in the single-sided geometry ($\varepsilon = 1$).

IV. Models

This section summarizes and categorizes the models used to predict the lift and the drag forces generated in PM-EDSs. They can be divided into two categories: global models, using equivalent circuits, and local models, starting from local formulations of Maxwell's equations. The performance and accuracy of both categories are often compared to

a reference model, generally based on finite-elements methods (FEM). When this is the case, the reference model is not developed as only the main model of each referred paper is presented.

A. Equivalent Circuit Models

These models start from the assumption that the currents induced in the discrete loops can be considered as filament currents, neglecting thus locally induced eddy currents, including the skin effect. By modeling the discrete loops with an equivalent circuit, it is possible to deduce the current in each loop from the electrical equation

$$\mathbf{V} = \mathbf{RI} + \mathbf{L}\frac{d\mathbf{I}}{dt} + \frac{d\mathbf{\Phi_0}}{dt} \tag{6}$$

where $\mathbf{R}$ and $\mathbf{L}$ are the resistance and inductance matrices of the loops, $\mathbf{\Phi_0}$ is the flux due to the PMs intercepted by the loops. By identification in the power balance of the system or using the magnetic coenergy, the forces can be computed, for this application, by

$$\mathbf{F} = \left[\frac{d\mathbf{\Phi_0}}{dx}\right]^T \mathbf{I}. \tag{7}$$

The forces can also be computed from the current and the magnetic flux density due to the PMs, $\mathbf{B_0}$, using the Lorentz force equation

$$d\mathbf{F} = i\,d\mathbf{l} \times \mathbf{B_0} \tag{8}$$

which is a more local approach since $\mathbf{B_0}$ needs to be evaluated on each loop.

The global parameters used in these equivalent circuits such as the resistance, the inductance, and the magnetic flux must be evaluated through the use of local models either analytical or numerical, presented in Section IV-B, or even with experimental data. A general formulation of the method with SCMs can be found in [79]. The authors computed the forces with the energy method. They also applied the theory to two topologies of discrete tracks: loop-shaped coils and eight-shaped null-flux coils.

Post and Ryutov [10], [36] considered an infinite 2-D magnetic field source with a sinusoidal magnetic flux linkage intercepted by filament loops. They made, at first, the following assumptions: only the self-inductance of the loops is considered, fixed levitation gap, steady state, and averaged forces. With their model, they found an expression of the LDR

$$\mathrm{LDR} = \frac{\omega L}{R}. \tag{9}$$

They then modeled the magnetic coupling between the loops through an added inductance.

Other researchers worked on the Inductrack concept. Murai and Hasegawa [37] described simulations using a 3-D Fourier-based approach to model the magnetic field source. To develop their transient model of the Inductrack, Wang and Yang [38] derived analytically the magnetic field of a nonsinusoidal Halbach array with finite dimensions using the Biot–Savart law.

de Boeij *et al.* [32] modeled eight-shaped coils using analytical expressions of the magnetic field of a PM, computed from a local model, and an equivalent circuit. They also derived a simpler algebraic model, considering an invariant magnetic field in the plane of the coils, more suited to real-time simulations. Both models are more computationally efficient than numerical methods and showed a good agreement with measurements.

Guo *et al.* [34] also worked on eight-shaped coils. They computed the mutual inductance between a single PM, modeled as a current loop, and the track with the Neumann formula. Very recently, Zhu *et al.* [35] developed a numerical calculation model of a multimagnet array and eight-shaped coils in a similar manner. In the latter, the PMs are discretized in coil groups and the forces are computed from the mutual inductance between these coils and the eight-shaped coils modeled as an equivalent circuit, as commonly done in the literature. In this circuit, two voltage sources, resistances, and mutually linked inductances are used to consider the upper and lower loops. However, it can be reduced to a circuit similar to the one in Fig. 4 with an equivalent source, resistance, and cyclic inductance when there is no cross-connection between the left and right coils of the guideway. Considering the edge effects, they found an average error of 16.58%, 11.03%, and 6.42% for the drag, levitation, and guidance forces between their model and 3-D FEM.

Storset and Paden [23] used a different approach. They derived equations for discrete tracks starting from a general diffusion equation describing the evolution of current fields in an arbitrary track. They also showed how the equations can be simplified with the filament currents approximation, to have equations similar to (6). From this, they derived simpler models considering a periodic track which are more computationally efficient [80].

Equivalent circuit models are mostly used in EDS systems with discrete tracks. However, Storset and Paden's approach [23] could have been generalized to continuous tracks. Another exception can be found in [24], where Galluzzi *et al.* used a lumped-parameter model to easily couple the mechanical and electromechanical domains in a continuous track. They used an equivalent circuit model with not one but several branches to take into account the impact of the speed on the distribution of the current in the conductive track. The values of the parameters were not computed analytically but fitted with finite-element simulations. They found that three branches is already a suitable choice for their case study.

B. Local Models

Local models start from a local formulation of Maxwell equations. Unlike the previous models, they are not well suited to transient analyses and are usually used under a quasi-static condition.

1) Numerical: Numerical models are based on FEM. They are generally built using software like FEMM, COMSOL Multiphysics, or ANSYS Maxwell. Allowing for fewer assumptions but being also more time consuming, they are mainly used in the literature to verify the results of analytical models or, to a lesser extent, to evaluate global parameters of analytical models based on circuit theory. In addition, they generally concern continuous tracks topologies since discrete tracks are

much more difficult to model because their discrete nature would require a full transient analysis to extract quasi-static features.

Íñiguez and Raposo [48] did a numerical study in 2-D using FEMM and compared it with experimental results. They found discrepancies between the two mainly because of the transverse edge effects they did not consider. Guo *et al.* [59] designed a side-wall mounted continuous track EDS in 3-D using ANSYS. With their model, the authors were able to conduct several analyses such as the eddy current distribution in the conductive plate, the impact of the magnet arrangement, or a parametric study on the different dimensions of the system. Kublin *et al.* [22] used Ansys Maxwell to conduct transient numerical simulations in 3-D of a Halbach array moving above a conductive plate. They adapted the plate length and the simulation time to have stabilized forces. They also determined a specific mesh density to limit the computation time and estimated the error of computation at around 5% due to this limit.

2) Analytical: Different kinds of analytical models were developed in the literature. The first and most used type is Fourier-based models. A general formulation of this method with the underlying assumptions can be found in [81]. The geometry is decomposed in regions characterized by a constant electrical conductivity and magnetic permeability. Maxwell equations can be then simplified in each region. In the conductor, they reduce to

$$\nabla^2 \mathbf{A} = \mu\sigma \mathbf{v} \times (\nabla \times \mathbf{A}) \tag{10}$$

where $\mathbf{A}$ is the magnetic vector potential and $\mathbf{v}$ is the relative velocity between the magnets and the guideway. In the PMs, they become

$$\nabla^2 \mathbf{A} = -\mu \nabla \times \mathbf{M} \tag{11}$$

$$\nabla^2 \phi = \frac{\nabla \cdot \mathbf{M}}{\mu} \tag{12}$$

where $\mathbf{M}$ is the magnetization of the PMs and ϕ is the magnetic scalar potential. Elsewhere, they simplify to a Laplace equation

$$\nabla^2 \mathbf{A} = \mathbf{0} \tag{13}$$

$$\nabla^2 \phi = 0. \tag{14}$$

The solutions of these equations are Fourier series involving coefficients which are found with the boundary conditions between regions. The forces can then be computed using either

$$\mathbf{F} = \int_V \mathbf{J} \times \mathbf{B_0} dV \tag{15}$$

where $\mathbf{J}$ is the current density in the track computed with Ampere's law and V is the volume of conductor, or using the Maxwell stress tensor simplified for magnetic problems

$$\mathbf{F} = \oint_S \boldsymbol{\sigma} \cdot \hat{n} dS \tag{16}$$

$$\sigma_{ij} \equiv \frac{1}{\mu_0}\left(B_i B_j - \frac{1}{2}\delta_{ij} B^2\right) \tag{17}$$

with $\hat{n}$ the vector normal to the integration surface.

Such models can be made in two or three dimensions, and consider or not the finite length and the finite width of the problem. Cho *et al.* [46] developed a 2-D Fourier-based model, without considering the edge effects, with the magnetic vector potential. These effects being far from negligible in their study case, the authors observed that the experimental data of the forces were only 60% of the 2-D model. Chen and Zhang [49], [50] proposed a 2-D model also based on the magnetic vector potential but showing a smaller error compared to a 3-D FEM simulation. However, this could be due to a PM width almost three times larger than its pole pitch, reducing the impact of the transverse edge effects. Hu *et al.* [20] obtained a 2-D model based on both the scalar and vector magnetic potentials. When comparing to 2-D and 3-D FEM, they showed that the edge effects in the longitudinal direction caused a drop of 10% in the forces while the edge effects in the transverse direction caused a drop of more than 50%, which matches the previous works. Flankl *et al.* [21] developed a simple 2-D model for an infinitely long and wide geometry and a given magnetic field in the air gap. With a 2-D FEM model, they then analyzed the impact on the drag-to-lift ratio of the edge effects and the discrete magnetization. The error between their scaling law for the drag-to-lift ratio and 3-D FEM was found to be less than 10%. Other authors derived 2-D models considering the finite length of the PMs [57], or not [17], showing a good accuracy compared to FEM simulations. Cho *et al.* [47] used a corrected conductivity in the plate to take into account its finite width in a 2-D model [82]. They compared their results to a 3-D FEM model and found an error of around 50% attributed to the transverse edge effects caused by the longitudinal component of eddy currents in the plate.

2-D analytical models, in general, have made possible the derivation of approximate but simple expressions for the LDR, illustrated in Fig. 7 and obtained with the same model as in Fig. 5. These are based on a distinction between thin and thick plates and between low and high speed, as stated by Hill [45] and Lee and Menendez [83]. In synthesis, if the thickness t_c of the conductor is smaller than (τ/π), then the plate is said to be thin. For such thin plates, the LDR expression depends on the value of δ_{skin} and thus the speed [42], [71], [84]–[86]. If $\delta_{\text{skin}} > t_c$, then the magnetic field penetrates inside the full conductor and the LDR is given by

$$\text{LDR}_1 = \frac{v}{w} \tag{18}$$

where $w = (2/\mu\sigma t_c)$ is Maxwell's recoil speed. If $\delta_{\text{skin}} < t_c$, then the eddy currents are confined in a layer of thickness δ_{skin} thinner than the conductor, leading to

$$\text{LDR}_2 = \frac{\tau}{\pi \delta_{\text{skin}}}. \tag{19}$$

In Fig. 7, all the LDR computed with the 2-D model converge, at high speed, toward the same asymptote, independent of the plate thickness. This asymptote is correctly modeled by LDR_2. At low speed, the LDR varies linearly with the speed but with the track thickness t_c as expected from LDR_1. However, when the plate thickness increases, it deviates from the asymptotic behavior and converges toward the same value. This is the

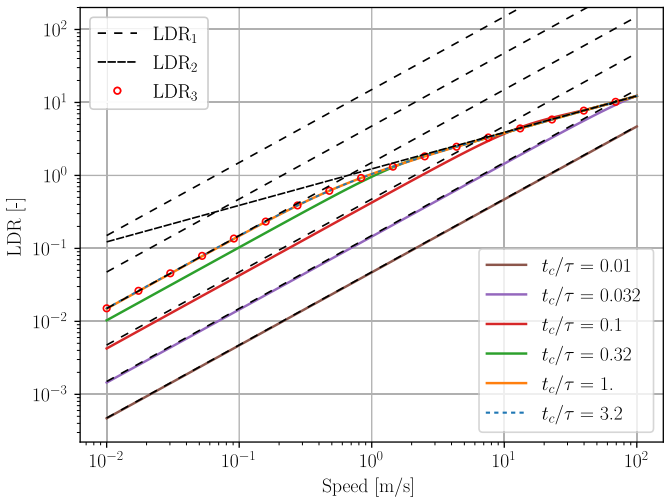

Fig. 7. LDR versus speed for different thicknesses of the conductive plate. The solid color lines are computed with a 2-D analytical model. Expressions of LDR_1, LDR_2, and LDR_3 are, respectively, given by (18)–(20).

thick plate limit where the thickness t_c of the conductor is larger than (τ/π). In this case, the magnetic field does not penetrate inside the full conductor, even at very low speed, and thus the LDR is independent of the plate thickness. For thick plates, when $\delta_{\mathrm{skin}} > (\tau/\pi)$, the ratio is then given by (18) but with (τ/π) instead of t_c. When $\delta_{\mathrm{skin}} < (\tau/\pi)$, the LDR remains the same as in thin plates by (19) since the eddy currents are confined in a layer thinner than the conductor. As illustrated in Fig. 7, the transition between low and high speed for thick plates obtained with the 2-D model is not well approximated by the asymptotes. However, an analytical expression of the LDR valid for the full speed range in thick plates exists and can be found in [36]

$$\mathrm{LDR}_3 = \frac{\tau}{\pi\,\delta_{\mathrm{skin}}}\sqrt{\sqrt{1+\frac{\pi^4\delta_{\mathrm{skin}}^4}{4\tau^4}}-\frac{\pi^2\delta_{\mathrm{skin}}^2}{2\tau^2}}. \tag{20}$$

To have better accuracy, 3-D analytical models were developed to consider edge effects in both longitudinal and transverse directions. Chen *et al.* [52] and Duan *et al.* [55] used the second-order vector potential (SOVP) instead of the first-order one to simplify the computations. They found a great agreement between their model and the experimental data. Tongyu and Dazhi [54] used a combination of the diffusion equation of the magnetic field in the conductive plate and the scalar potential in all the other regions. Without considering the finite length of the PM array in the longitudinal direction in their model, they also obtained an error below 5% between analytical and experimental results.

Other types of analytical models were developed for different purposes. Ko and Ham [87] proposed a model based on wavelet transform. The functions are developed in terms of wavelets and not trigonometric polynomials to capture the transient response of EDS systems, which is different than the other local models based on a quasi-static condition. Hill [45] solved the magnetic flux density diffusion equation in the conductor without using magnetic potentials. He considered a 2-D problem with no edge effects while modeling the magnetic field source as a sinusoidally distributed current sheet. He then found a simpler expression of the forces considering a thin conductive plate. Vaez-Zadeh and Hossein [51] and Hasanzadeh *et al.* [53] modeled a single magnet as current sheets, computed the magnetic field in the track due to these current sheets limited to its fundamental component, and then combined it with the expressions of the forces developed by Hill. Finally, some older research (see [42], [84]) used the thin plate theory based on the method of images developed by Maxwell. The theory was well explained by Davis and Reitz [88]. The instantaneous eddy current field due to a magnetic source moving relative to a conductor can be visualized as being produced by a pair of images with opposite signs, one located below the source and one below the previous position of the source with an opposite sign. The eddy current decay is modeled by the image pair moving away from the sheet at a speed equal to Maxwell's recoil speed. *Hence a moving magnet leaves behind it a "trail of receding images"* [88]. At the very high speed limit, *the magnet moves away from its trail of eddy currents before they can decay appreciably*. The lift force can be then approximated as the one between the real magnet and its image below the sheet. This phenomenon is also explained in the following way. At very high speed, the induced eddy currents produce a magnetic field nearly equal to one that generated them, without any losses [12], [44].

V. Experimental Setups

To validate the concepts but mainly the models of PM-EDS topologies, authors built experimental setups.

To be able to measure the performance of small-scale experimental setups at high speed without requiring large and expensive infrastructures, rotary test rigs were developed with two distinct configurations.

In the first configuration, represented in Fig. 8 for a *null-flux* topology, the conductive track has a disk shape and the PM arrangement develops an axial magnetic field so as to experience an axial lift force. Chen *et al.* [52] and Duan *et al.* [55] used such an experimental setup to validate their model of *null-flux* PM-EDS. Their device, made of a 3-mm-thick aluminum conductive plate with a radius of 50 cm rotating between two Halbach arrays, can reach 25 m/s. A similar test rig with a maximum rotational velocity of 20 m/s was used by Kratz and Post [39] but with a copper wheel made of 100 radially oriented wires between a copper disk hub and an external ring, to simulate a ladder-type track. Tongyu and Donzhi [54] developed a disk-type testbench for a *normal-flux* topology with a diameter of 23 cm and going up to 10 m/s. Recently, Hu *et al.* [20] used an experimental device ensuring a speed of 60 m/s with a 30-mm-thick aluminum disk with a radius of 0.35 m. The lift and drag forces were measured by two forces sensors positioned along the y-axis and x-axis, respectively.

In the second configuration, represented in Fig. 9, the conductive track is a drum and the PM arrangement develops a radial magnetic field so as to experience a radial lift force. Cho *et al.* [46] and Cho *et al.* [47] used a setup made of

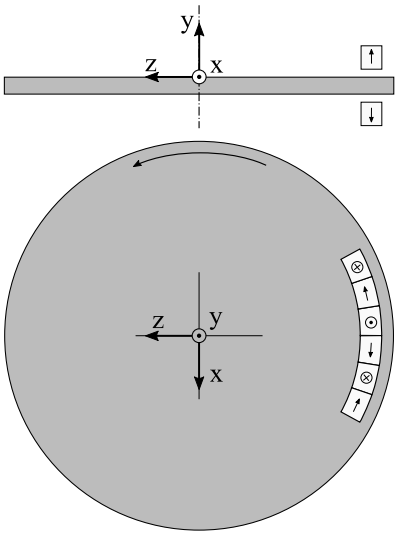

Fig. 8. Disk-type rotary experimental setup. The levitation direction is along the *y*-axis. The European method of projection views has been used.

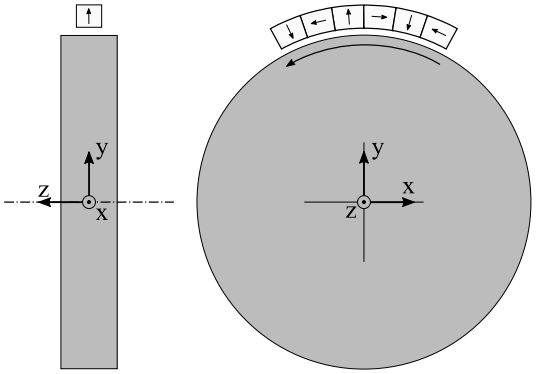

Fig. 9. Drum-type rotary experimental setup. The levitation direction is along the *y*-axis. The European method of projection views has been used.

a rotary wheel with a diameter of 1.5 m with a 262-mm-wide and 35-mm-thick aluminum plate mounted on its outer surface. This device was able to simulate a linear velocity up to 150 m/s. Íñiguez and Raposo [48] developed a much smaller setup based on the same principle but with a 15-mm-thick outer rim made of copper. The maximum tangential speed was 8–10 m/s, the topic of the article being the study of a low-speed model. The setup presented in [51] and [53] is made of a rotating aluminum cylinder but with a single magnet. Their measurements went up to 35 m/s.

In addition to these rotary test rigs, some linear setups were also developed, like the one built by the MIT Hyperloop team [15]. On a 23-m-long track, their small cart equipped with magnets and load cells was able to reach a speed of 20 m/s. The results obtained with this setup were in good agreement with their simulations. Other linear setups were developed for the Inductrack concept. The first one is a small-scale setup with a 20-m-long array of coils which are 15 cm wide [89]. Auxiliary wheels are attached to the cart and ride on aluminum-channel rails on the side of the coils. The authors observed a stable levitation flight of the cart down the track when it was mechanically launched at a speed above 2 m/s. The second one, based on the same topology, is made of a 7.8-m track and 9-kg cradle. The drag force was higher than expected, preventing them to test correctly their Inductrack NASA model rocket launcher [90]. The last one is a full-scale test track developed for the General Atomics Urban Maglev Program [13]. The ladder-type track is 120 m long and made of Litz wire. The vehicle is equipped with a *null-flux* arrangement of Halbach arrays.

VI. Conclusion

This article reviewed the different topologies of PM-EDSs developed during the past years. They were classified depending on their magnetic field source and their track, and an explanation of the working principle was given for the different types of tracks. This article also presented the various models, global or local and, for the latter, numerical or analytical, used to predict the quasi-static performance of PM-EDSs. A summary of the LDR expressions obtained with simple models for different types of tracks was presented, highlighting the dimensions and speed dependencies. Finally, the main experimental setups used to validate the concepts and the models of the topologies described in this article were listed.

As seen in this review, a lot of interest has been given to PM-EDSs through the years but there is still no real integration of this type of suspension in MAGLEV transportation systems. However, most of the research efforts have been limited to studying specific PM-EDS topologies, sometimes comparing their performance with another one. There is therefore a need for a global comparison between the existing topologies, which could help select a specific type of PM-EDS for a given application. The criteria on the basis of which to compare these topologies are also a point that deserves particular attention. Indeed, beyond the commonly used LWR and LDR, other criteria like the environmental or economical costs would help conduct a fair comparison, encompassing more aspects of the PM-EDS system and its applications such as the complete journey of the vehicle, the time of operation or the production costs. Beyond that, the advent of EDSs will require studies on their integration in the vehicles and interaction with the other components of a MAGLEV transport system, such as the propulsion, the external guidance if any, or the landing system.

References

[1] K. van Goeverden, B. van Arem, and R. van Nes, "Volume and GHG emissions of long-distance travelling by western Europeans," *Transp. Res. D, Transp. Environ.*, vol. 45, pp. 28–47, Jun. 2016.
[2] *Hyperloop Alpha*, SpaceX, Hawthorne, CA, USA, 2013.
[3] E. Chaidez, S. P. Bhattacharyya, and A. N. Karpetis, "Levitation methods for use in the hyperloop high-speed transportation system," *Energies*, vol. 12, no. 21, p. 4190, Nov. 2019.
[4] H.-W. Lee, K.-C. Kim, and J. Lee, "Review of Maglev train technologies," *IEEE Trans. Magn.*, vol. 42, no. 7, pp. 1917–1925, Jul. 2006.
[5] H.-S. Han and D.-S. Kim, *Magnetic Levitation* (Springer Tracts on Transportation and Traffic), vol. 13. Dordrecht, The Netherlands: Springer, 2016.
[6] Z. Long, G. He, and S. Xue, "Study of EDS & EMS hybrid suspension system with permanent-magnet Halbach array," *IEEE Trans. Magn.*, vol. 47, no. 12, pp. 4717–4724, Dec. 2011.

[7] Z. Deng *et al.*, "A high-temperature superconducting maglev-evacuated tube transport (HTS maglev-ETT) test system," *IEEE Trans. Appl. Supercond.*, vol. 27, no. 6, pp. 1–8, Sep. 2017.

[8] R. M. R. Stephan de Andrade, Jr., and A. C. G. G. F. Sotelo, "Superconducting levitation applied to urban transportation," in *Wiley Encyclopedia of Electrical and Electronics Engineering*. Hoboken, NJ, USA: Wiley 2017, pp. 1–18.

[9] J. Z. Bird, "A review of integrated propulsion, suspension and guidance passive guideway maglev technologies," in *Proc. 12th Int. Symp. Linear Drives Ind. Appl. (LDIA)*, Jul. 2019, pp. 1–6.

[10] R. F. Post and D. D. Ryutov, "The inductrack: A simpler approach to magnetic levitation," *IEEE Trans. Appl. Supercond.*, vol. 10, no. 1, pp. 901–904, Mar. 2000.

[11] J. K. Noland, "Prospects and challenges of the hyperloop transportation system: A systematic technology review," *IEEE Access*, vol. 9, pp. 28439–28458, 2021.

[12] T. N. Franca, H. Shi, Z. Deng, and R. M. Stephan, "Overview of electrodynamic levitation technique applied to maglev vehicles," *IEEE Trans. Appl. Supercond.*, vol. 31, no. 8, pp. 1–5, Nov. 2021.

[13] S. Gurol, R. Baldi, D. Bever, and R. Post, "Status of the general atomics low speed urban maglev technology development program," in *Proc. 18th Int. Conf. Magnetically Levitated Syst. Linear Drives*, Shanghai, China, Oct. 2004, pp. 269–274.

[14] S. Sadeghi, M. Saeedifard, and C. Bobko, "Dynamic modeling and simulation of propulsion and levitation systems for hyperloop," in *Proc. 13th Int. Symp. Linear Drives Ind. Appl. (LDIA)*, Jul. 2021, pp. 1–5.

[15] *MIT Hyperloop Final Report*, MIT, Cambridge, MA, USA, 2017.

[16] D. M. Rote and Y. Cai, "Review of dynamic stability of repulsive-force maglev suspension systems," *IEEE Trans. Magn.*, vol. 38, no. 2, pp. 1383–1390, Mar. 2002.

[17] M. Zhao, Q. Ge, Z. Gao, Y. Zheng, B. Zhang, and X. Cao, "Analysis of electromagnetic and damping characteristics of permanent magnet electrodynamic suspension system," in *Proc. 13th Int. Symp. Linear Drives Ind. Appl. (LDIA)*, Jul. 2021, pp. 1–6.

[18] Q. Han, "Analysis and modeling of the EDS maglev system based on the Halbach permanent magnet array," Ph.D. dissertation, Dept. Elect. Comput. Eng., Univ. Central Florida, Orlando, FL, USA, 2004.

[19] C. Luo, K. Zhang, J. Duan, and Y. Jing, "Study of permanent magnet electrodynamic suspension system with a novel Halbach array," *J. Electr. Eng. Technol.*, vol. 15, no. 2, pp. 969–977, Mar. 2020.

[20] Y. Hu, Z. Long, J. Zeng, and Z. Wang, "Analytical optimization of electrodynamic suspension for ultrahigh-speed ground transportation," *IEEE Trans. Magn.*, vol. 57, no. 8, pp. 1–11, Aug. 2021.

[21] M. Flankl, T. Wellerdieck, A. Tüysüz, and J. W. Kolar, "Scaling laws for electrodynamic suspension in high-speed transportation," *IET Elect. Power Appl.*, vol. 12, no. 3, pp. 357–364, Nov. 2018.

[22] T. Kublin, L. Grzesiak, P. Radziszewski, M. Nikoniuk, and Ł. Ordyszewski, "Reducing the power consumption of the electrodynamic suspension levitation system by changing the span of the horizontal magnet in the Halbach array," *Energies*, vol. 14, no. 20, p. 6549, Oct. 2021.

[23] O. F. Storset and B. E. Paden, "Discrete track electrodynamic maglev Part I: Modelling," *IEEE Trans. Magn.*, 2005.

[24] R. Galluzzi *et al.*, "A multi-domain approach to the stabilization of electrodynamic levitation systems," *J. Vib. Acoust.*, vol. 142, no. 6, May 2020, Art. no. 061004.

[25] J. Van Verdeghem, M. Lefebvre, V. Kluyskens, and B. Dehez, "Dynamical modeling of passively levitated electrodynamic thrust self-bearing machines," *IEEE Trans. Ind. Appl.*, vol. 55, no. 2, pp. 1447–1460, Mar. 2019.

[26] J. R. Powell and G. T. Danby, "Electromagnetic inductive suspension and stabilization system for a ground vehicle," U.S. Patent 3 470 828A, Oct. 7, 1969.

[27] K. R. Davey, "Designing with null flux coils," *IEEE Trans. Magn.*, vol. 33, no. 5, pp. 4327–4334, Sep. 1997.

[28] Y. Cai *et al.*, "Semianalytical calculation of superconducting electrodynamic suspension train using figure-eight-shaped ground coil," *IEEE Trans. Appl. Supercond.*, vol. 30, no. 5, pp. 1–9, Aug. 2020.

[29] J. Lim, C.-Y. Lee, J.-H. Lee, W. You, K.-S. Lee, and S. Choi, "Design model of null-flux coil electrodynamic suspension for the hyperloop," *Energies*, vol. 13, no. 19, p. 5075, Sep. 2020.

[30] T. Gong, G. Ma, R. Wang, S. Li, C. Yao, and L. Xiao, "3-D FEM modeling of the superconducting EDS train with cross-connected figure-eight-shaped suspension coils," *IEEE Trans. Appl. Supercond.*, vol. 31, no. 3, pp. 1–13, Apr. 2021.

[31] G. Ma, Y. Wang, J. Luo, Y. Cai, R. Wang, and X. Song, "An analytical-experiment coupling method to characterize the electrodynamic suspension system at various speeds," *IEEE Trans. Ind. Electron.*, vol. 69, no. 7, pp. 7170–7180, Jul. 2022.

[32] J. de Boeij, M. Steinbuch, and H. M. Gutierrez, "Modeling the electromechanical interactions in a null-flux electrodynamic maglev system," *IEEE Trans. Magn.*, vol. 41, no. 1, pp. 466–470, Jan. 2005.

[33] T. N. Franca, H. Shi, Z. Deng, and R. M. Stephan, "Study of a null-flux suspension system using permanent magnet Halbach arrays," in *Proc. IEEE Int. Conf. Appl. Supercond. Electromagn. Devices (ASEMD)*, Oct. 2020, pp. 1–2.

[34] Guo, Li, and Zhou, "Study of a null-flux coil electrodynamic suspension structure for evacuated tube transportation," *Symmetry*, vol. 11, no. 10, p. 1239, Oct. 2019.

[35] H. Zhu, H. Huang, J. Zheng, H. Shi, Y. Xiang, and K. Li, "A numerical calculation model of multi-magnet-array and 8-shaped null-flux coil for permanent magnet EDS vehicle system," *IEEE Trans. Magn.*, vol. 58, no. 5, pp. 1–11, May 2022.

[36] R. F. Post and D. Ryutov, "The Inductrack concept: A new approach to magnetic levitation," Lawrence Livermore National Lab. (LLNL), Livermore, CA, USA, Tech. Rep. UCRL-ID-124115, May 1996.

[37] T. Murai and H. Hasegawa, "Electromagnetic analysis of inductrack magnetic levitation," *Electr. Eng. Jpn.*, vol. 142, no. 1, pp. 67–74, Jan. 2003.

[38] R. Wang and B. Yang, "Transient response of Inductrack systems for maglev transport: Part I—A new transient model," *J. Vib. Acoust.*, vol. 142, no. 3, pp. 1–24, Jun. 2020.

[39] R. Kratz and R. F. Post, "A null-current electro-dynamic levitation system," *IEEE Trans. Appl. Supercond.*, vol. 12, no. 1, pp. 930–932, Mar. 2002.

[40] T. Yamada, M. Iwamoto, and T. Ito, "Levitation performance of magnetically suspended high speed trains," *IEEE Trans. Magn.*, vol. MAG-8, no. 3, pp. 634–635, Sep. 1972.

[41] T. Akinbiyi, P. Burke, and B. Ooi, "A comparison of ladder and sheet guideways for electrodynamic levitation of high speed vehicles," *IEEE Trans. Magn.*, vol. MAG-12, no. 6, pp. 879–881, Nov. 1976.

[42] W. M. Saslow, "Maxwell's theory of eddy currents in thin conducting sheets, and applications to electromagnetic shielding and MAGLEV," *Amer. J. Phys.*, vol. 60, pp. 693–771, Aug. 1992.

[43] H. A. Wheeler, "Formulas for the skin effect," *Proc. IRE*, vol. 30, no. 9, pp. 412–424, Sep. 1942.

[44] L. Hao, Z. Huang, F. Dong, D. Qiu, B. Shen, and Z. Jin, "Study on electrodynamic suspension system with high-temperature superconducting magnets for a high-speed maglev train," *IEEE Trans. Appl. Supercond.*, vol. 29, no. 2, pp. 1–5, Mar. 2019.

[45] R. J. Hill, "Teaching electrodynamic levitation theory," *IEEE Trans. Educ.*, vol. 33, no. 4, pp. 346–354, Nov. 1990.

[46] H. Cho, D. K. Bae, H. K. Sung, and J. Lee, "Experimental study on the electrodynamic suspension system with HTSC and PM Halbach array magnets," *IEEE Trans. Appl. Supercond.*, vol. 18, no. 2, pp. 808–811, Jun. 2008.

[47] H.-W. Cho, H.-S. Han, J.-S. Bang, H.-K. Sung, and B.-H. Kim, "Characteristic analysis of electrodynamic suspension device with permanent magnet Halbach array," *J. Appl. Phys.*, vol. 105, no. 7, 2009, Art. no. 07A314.

[48] J. Ìñiguez and V. Raposo, "Numerical simulation of a simple low-speed model for an electrodynamic levitation system based on a Halbach magnet array," *J. Magn. Magn. Mater.*, vol. 322, nos. 9–12, pp. 1673–1676, May 2010.

[49] Y. Chen and K. L. Zhang, "Calculation and analysis of the forces created by Halbach permanent-magnet electrodynamic suspension," *Appl. Mech. Mater.*, vols. 229–231, pp. 440–443, Nov. 2012.

[50] Y. Chen and K. Zhang, "Electromagnetic force calculation of conductor plate double Halbach permanent magnet electrodynamic suspension," *ACES J.*, vol. 29, no. 11, p. 7, 2014.

[51] H. Rezaei and S. Vaez-Zadeh, "Modelling and analysis of permanent magnet electrodynamic suspension systems," *Prog. Electromagn. Res. M*, vol. 36, pp. 77–84, 2014.

[52] Y. Chen, W. Zhang, J. Z. Bird, S. Paul, and K. Zhang, "A 3-D analytic-based model of a null-flux Halbach array electrodynamic suspension device," *IEEE Trans. Magn.*, vol. 51, no. 11, pp. 1–5, Nov. 2015.

[53] S. Hasanzadeh, H. Rezaei, and E. Qiyassi, "Analysis and optimization of permanent magnet dimensions in electrodynamic suspension systems," *J. Electr. Eng. Technol.*, vol. 13, no. 1, pp. 307–314, 2018.

[54] S. Tongyu and W. Dazhi, "3D analytical model of drag and lift force for a conductive plate moving above a Halbach magnet array," *Trans. Inst. Meas. Control*, vol. 40, no. 12, pp. 3515–3524, 2018.
[55] J. Duan, S. Xiao, K. Zhang, M. Rotaru, and J. K. Sykulski, "Analysis and optimization of asymmetrical double-sided electrodynamic suspension devices," *IEEE Trans. Magn.*, vol. 55, no. 6, pp. 1–5, Jun. 2019.
[56] C. Luo, K. Zhang, W. Zhang, and Y. Jing, "3D analytical model of permanent magnet and electromagnetic hybrid Halbach array electrodynamic suspension system," *J. Electr. Eng. Technol.*, vol. 15, no. 4, pp. 1713–1721, Jul. 2020.
[57] F. Wang, J. Zhang, J. Zhao, and W. Qin, "Two dimensional analytical modeling and electromagnetic force optimization of permanent magnet electrodynamic suspension system," in *Proc. 13th Int. Symp. Linear Drives Ind. Appl. (LDIA)*, Jul. 2021, pp. 1–5.
[58] H. Wang and J. Nengqiang, "Research in the multilayer sheet guildways of Maglev," in *Proc. 6th Int. Conf. Electr. Mach. Syst. (ICEMS)*, Beijing, China, Nov. 2003, pp. 941–943.
[59] Z. Guo, D. Zhou, Q. Chen, P. Yu, and J. Li, "Design and analysis of a plate type electrodynamic suspension structure for ground high speed systems," *Symmetry*, vol. 11, no. 9, p. 1117, Sep. 2019.
[60] J. Bird and T. A. Lipo, "The experimental verification of the lift, thrust and guidance forces created by an electrodynamic wheel rotating over a split-sheet guideway," in *Proc. 19th Int. Conf. Magnetically Levitated Syst. Linear Drives*, Dresden, Germany, 2006, pp. 1–9.
[61] D. L. Atherton and A. R. Eastham, "Flat guidance schemes for magnetically levitated high-speed guided ground transport," *J. Appl. Phys.*, vol. 45, no. 3, pp. 1398–1405, Mar. 1974.
[62] T. Sakamoto, A. R. Eastham, and G. E. Dawson, "Induced currents and forces for the split-guideway electrodynamic levitation system," *IEEE Trans. Magn.*, vol. 27, no. 6, pp. 5004–5006, Nov. 1991.
[63] H. H. Kolm, R. D. Thornton, Y. Iwasa, and W. S. Brown, "The magneplane system," *Cryogenics*, vol. 15, no. 7, pp. 377–384, Jul. 1975.
[64] D. B. Montgomery, "Overview of the 2004 Magplane design," in *Proc. 18th Int. Conf. Magnetically Levitated Syst. Linear Drives*, Shanghai, China, 2004, p. 106.
[65] N. Fujii, G. Hayashi, and Y. Sakamoto, "Characteristics of magnetic lift, propulsion and guidance by using magnet wheels with rotating permanent magnets," in *Proc. 35th IAS Annu. Meeting World Conf. Ind. Appl. Electr. Energy*, Rome, Italy, vol. 1, 2000, pp. 257–262.
[66] K. Davey, "Optimization shows Halbach arrays to be non-ideal for induction devices," *IEEE Trans. Magn.*, vol. 36, no. 4, pp. 1035–1038, Jul. 2000.
[67] W. Jiangbo, L. Chunsheng, X. Wei, and Y. Baofeng, "Optimization design of linear Halbach array for EDS maglev," in *Proc. IEEE Vehicle Power Propuls. Conf.*, Sep. 2008, pp. 1–5.
[68] Q. Han, C. Ham, and R. Phillips, "Four- and eight-piece Halbach array analysis and geometry optimisation for maglev," *IEE Proc.-Electric Power Appl.*, vol. 152, no. 3, pp. 535–542, May 2005.
[69] C. Ham, W. Ko, and Q. Han, "Analysis and optimization of a Maglev system based on the Halbach magnet arrays," *J. Appl. Phys.*, vol. 99, no. 8, Apr. 2006, Art. no. 08P510.
[70] J. Hogan and H. Fink, "Comparison and optimization of lift and drag forces on vehicles levitated by eddy current repulsion for various null and normal flux magnets with one or two tracks," *IEEE Trans. Magn.*, vol. MAG-11, no. 2, pp. 604–607, Mar. 1975.
[71] P. L. Richards and M. Tinkham, "Magnetic suspension and propulsion systems for high-speed transportation," *J. Appl. Phys.*, vol. 43, pp. 2680–2691, Jan. 1972.
[72] J. Miericke and L. Urankar, "Theory of electrodynamic levitation with a continuous sheet track—Part I," *Applied Phys.*, vol. 2, no. 4, pp. 201–211, Oct. 1973.
[73] H. Hieronymus, J. Miericke, F. Pawlitschek, and M. Rudel, "Experimental study of magnetic forces on normal and null flux coil arrangements in the inductive levitation system," *Appl. Phys.*, vol. 3, no. 5, pp. 359–366, May 1974.
[74] W. Qin, M. Yuhua, L. Gang, W. Fuyao, S. Chengrui, and Z. Jielong, "Investigation of asymmetric axial-flux hybrid excited electrodynamic wheels for maglev transportation," in *Proc. IEEE Energy Convers. Congr. Expo. (ECCE)*, Vancouver, BC, Canada, Oct. 2021, pp. 3753–3758.
[75] J. Bird and T. A. Lipo, "An electrodynamic wheel: An integrated propulsion and levitation machine," in *Proc. IEEE Int. Electr. Mach. Drives Conf.*, vol. 3, Jan. 2003, pp. 1410–1416.
[76] J. Bird and T. A. Lipo, "Calculating the forces created by an electrodynamic wheel using a 2-D steady-state finite-element method," *IEEE Trans. Magn.*, vol. 44, no. 3, pp. 365–372, Mar. 2008.
[77] J. Bird and T. A. Lipo, "A 3-D magnetic charge finite-element model of an electrodynamic wheel," *IEEE Trans. Magn.*, vol. 44, no. 2, pp. 253–265, Feb. 2008.
[78] X. Sang *et al.*, "Analysis and experiment on the levitation force and thrust force characteristics of a permanent magnet electrodynamic wheel for maglev car application," *IEEE Trans. Appl. Supercond.*, vol. 31, no. 8, pp. 1–4, Nov. 2021.
[79] J. Liang He, D. M. Rote, and H. T. Coffey, "Applications of the dynamic circuit theory to Maglev suspension systems," *IEEE Trans. Magn.*, vol. 29, no. 6, pp. 4153–4164, Nov. 1993.
[80] O. F. Storset and B. E. Paden, "Electrodynamic magnetic levitation with discrete track Part II: Periodic track model for numerical simulation and lumped parameter model," *IEEE Trans. Magn.*, 2005.
[81] B. L. J. Gysen, K. J. Meessen, J. J. H. Paulides, and E. A. Lomonova, "General formulation of the electromagnetic field distribution in machines and devices using Fourier analysis," *IEEE Trans. Magn.*, vol. 46, no. 1, pp. 39–52, Jan. 2010.
[82] J. D. Edwards, B. V. Jayawant, W. R. C. Dawson, and D. T. Wright, "Permanent-magnet linear eddy-current brake with a non-magnetic reaction plate," *IEE Proc.-Electr. Power Appl.*, vol. 146, no. 6, p. 627, 1999.
[83] S. W. Lee and R. Menendez, "Forces at low- and high–speed limits in magnetic levitation systems," *J. Appl. Phys.*, vol. 46, no. 1, pp. 422–425, Jan. 1975.
[84] J. R. Reitz, "Forces on moving magnets due to eddy currents," *Appl. Phys.*, vol. 41, no. 5, pp. 2067–2071, Apr. 1970.
[85] J. R. Reitz and L. C. Davis, "Force on a rectangular coil moving above a conducting slab," *Appl. Phys.*, vol. 43, no. 4, pp. 1547–1553, Apr. 1972.
[86] D. C. Burnham, "Asymptotic lift-to-drag ratios for magnetic suspension systems," *J. Appl. Phys.*, vol. 42, no. 9, pp. 3455–3457, Aug. 1971.
[87] W. Ko and C. Ham, "A novel approach to analyze the transient dynamics of an electrodynamics suspension maglev," *IEEE Trans. Magn.*, vol. 43, no. 6, pp. 2603–2605, Jun. 2007.
[88] L. C. Davis and J. R. Reitz, "Eddy currents in finite conducting sheets," *J. Appl. Phys.*, vol. 42, no. 11, pp. 4119–4127, Oct. 1971.
[89] R. Post, "Inductrack demonstration model," LLNL, Livermore, CA, USA, Tech. Rep. UCRL-ID–129664, Feb. 1998.
[90] L. S. Tung, R. F. Post, and J. Martinez-Frias, "Final progress report for the NASA inductrack model rocket launcher at the Lawrence Livermore national laboratory," LLNL, Livermore, CA, USA, Tech. Rep. UCRLID-144455, 2001.

Louis Beauloye was born in Belgium in 1999. He received the master's degree in electromechanical engineering from the Université catholique de Louvain (UCLouvain), Louvain-la-Neuve, Belgium, in 2021, where he is currently pursuing the Ph.D. degree with the Mechatronic, Electrical Energy, and Dynamic Systems Department.

He is also a Research Fellow with the Fonds de la Recherche Scientifique (FNRS), Brussels, Belgium. His research interests include magnetic levitation, and particularly permanent magnet electrodynamic suspensions.

Bruno Dehez (Senior Member, IEEE) was born in Belgium in 1975. He received the master's degree in electromechanical engineering and the Ph.D. degree from the Université catholique de Louvain (UCLouvain), Louvain-la-Neuve, Belgium, in 1998 and 2004, respectively.

He is currently a Professor with the Ecole Polytechnique de Louvain, UCLouvain. His research interests include the design, the modeling, and the optimization of all types of electromagnetic devices, ranging from superconducting magnets to electrical motors, and including magnetic bearings and gears. Among these, he is particularly interested in electrodynamic and permanent magnet (PM) bearings, high-performance PM machines, and their combination into self-bearing machines.